Old Dominion University Research Foundation

DEPARTMENT OF MECHANICAL ENGINEERING & MECHANICS
COLLEGE OF ENGINEERING & TECHNOLOGY
OLD DOMINION UNIVERSITY
NORFOLK, VIRGINIA 23529

GROUND-BASED TESTING OF THE DYNAMICS OF FLEXIBLE SPACE STRUCTURES USING BAND MECHANISMS

By

L. F. Yang, Graduate Research Assistant

and

Meng-Sang Chew, Principal Investigator

Progress Report
For the period ended March 15, 1991

Prepared for
National Aeronautics and Space Administration
Goddard Space Flight Center
Greenbelt, Maryland 20771

Under
Research Grant NAG-1-1117
Dr. Jer-Nan Juang, Technical Monitor
SDYD-Spacecraft Dynamics Branch

May 1991

Old Dominion University Research Foundation is a not-for-profit corporation closely affiliated with Old Dominion University and serves as the University's fiscal and administrative agent for sponsored programs.

Any questions or comments concerning the material contained in this report should be addressed to:

Executive Director
Old Dominion University Research Foundation
P. O. Box 6369
Norfolk, Virginia 23508-0369

Telephone: (804) 683-4293
Fax Number: (804) 683-5290

DEPARTMENT OF MECHANICAL ENGINEERING & MECHANICS
COLLEGE OF ENGINEERING & TECHNOLOGY
OLD DOMINION UNIVERSITY
NORFOLK, VIRGINIA 23529

GROUND-BASED TESTING OF THE DYNAMICS OF FLEXIBLE SPACE STRUCTURES USING BAND MECHANISMS

By

L. F. Yang, Graduate Research Assistant

and

Meng-Sang Chew, Principal Investigator

Progress Report
For the period ended March 15, 1991

Prepared for
National Aeronautics and Space Administration
Goddard Space Flight Center
Greenbelt, Maryland 20771

Under
Research Grant NAG-1-1117
Dr. Jer-Nan Juang, Technical Monitor
SDYD-Spacecraft Dynamics Branch

Submitted by the
Old Dominion University Research Foundation
P.O. Box 6369
Norfolk, Virginia 23508-0369

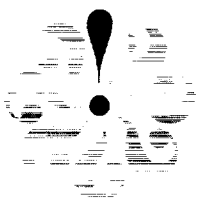

May 1991

ACKNOWLEDGMENTS

This is a progress report for the research project entitled "Investigation of Novel Suspension Systems for Ground-Based Testing of Flexible Space Structures" for the period ended March 15, 1991. This work was supported by the NASA Langley Research Center through research grant NAG-1-1117 and monitored by Dr. Jer-Nan Juang, of the SDYS, Spacecraft Dynamics Branch, NASA Langley Research Center, Mail Stop 297.

GROUND-BASED TESTING OF THE DYNAMICS OF FLEXIBLE SPACE STRUCTURES USING BAND MECHANISMS

L.F. Yang*

M. Chew**

Dept. of Mechanical Engineering and Mechanics

Old Dominion University

Norfolk, Virginia 23529-0247

J.N. Juang***

NASA Langley Research Center

Hampton, Virginia 23665

ABSTRACT

A suspension system based on a band mechanism is investigated to provide the free-free conditions for ground-based validation testing of flexible space structures. The band-mechanism consists of a noncircular disk with a convex profile, preloaded by torsional springs at its center of rotation so that static equilibrium of the test structure is maintained at any vertical location; the gravitational force will be directly counteracted during dynamic testing of the space structure. This noncircular disk within the suspension system can be configured to remain unchanged for test articles with the different weights as long as the torsional spring is replaced to maintain the originally designed frequency ratio of W/k_s. Simulations of test articles which are modelled as lumped-parameter as well as continuous parameter systems, will also be presented.

---

* Graduate Research Assistant. ** Associate Professor; Member, ASME.

*** Principal Scientist.

1. INTRODUCTION

Satellites have generally been treated dynamically as rigid bodies during their mission operations. However, interest in orbiting very large space structures has resulted in the need to maneuver and control flexible structures. This need is driving research into both dynamic analysis and experimental verification of large flexible space structures under zero-gravity. Several large flexible space structures presently under investigation includes the Mobile Satellite, the Large Deployable Reflector, the Freedom Space Station and other SDI weapon systems. These flexible space structures form the basis for much of present need for various forms of preflight testing and analysis on the ground.

A zero-gravity suspension environment is needed on the ground for dynamic testing of low-frequency flexible space structures. Several suspension devices [1-7] have been proposed in recent years. Figure 1 shows a band mechanism that will be applied as a suspension system. The dynamic interaction between this system and the test article forms the basis of investigation that is reported in this paper. The system features a noncircular disk, around which a cable winds and unwinds as the disk rotates. This disk has a special profile designed in conjunction with the load it is to suspend, as well as the spring stiffness of the torsional spring. The torsional spring loads the disk as the latter rotates so that the torque exerted by the spring about the disk axis of rotation is exactly counterbalanced by the force exerted by the weight of the test article on the cable that winds around the disk. In this way, the suspension system is capable of keeping the test structure in static equilibrium at any vertical location so that, on a static basis, the weightless effect of a test structure in space can be simulated on earth through this suspension system. A constraint on the system is that the profile

of disk must be convex to allow the cable to wind around its edge.

Two test articles have been selected for this investigation. The first test article, which consists of two masses and one linear connecting spring, is suspended from an equilibrium position. Such a lumped-parameter system is thus treated as a simple two-degree-of-freedom discrete system whose flexibility is characterized by the connecting spring. Another test article is a flexible steel beam which is hung at its two ends in equilibrium through two identical band drive suspension mechanisms. Simulation of the suspension system with the test articles originally at rest, are carried out with excitations such as an initial displacement and an initial velocity (impulse) on the masses. The characteristics of the flexible space structures are then analyzed in conjunction with this band drive suspension system.

2. EXISTING SUSPENSION SYSTEMS

Flexible space structures, in general, experience free-free boundary conditions that are not readily replicable on earth. Yet, to conduct the testing of such space structures, special devices must be introduced. These devices are to support the weight of structure without introducing any constraint forces which in turn impose boundary conditions that do not simulate the desired free-free boundary conditions in space. Several existing approaches and devices [1-7] have been used or proposed for suspending space structures for dynamic testing. Some of these are discussed below:

(1) Long Cables:

The space structure is suspended from a high ceiling through several long cables. Testing of the dynamics of the structure is conducted on a horizontal plane so as to reduce

the gravitational effect on the dynamics of the structure. The overhead suspension system for the Langley Lunar Landing Research Facility is a typical long-cable system designed to support five-sixths of the weight of the Apollo Lunar Lander Training Module.

(2) Air Pads:

Various designs based on the principle of reducing or eliminating friction on the horizontal plane had been proposed. Most common of which is the use of air pads that acts as hydrostatic air bearings on which the structure is suspended. Again, in such a design, the dynamic testing of the structure is conducted on a horizontal plane.

(3) Pneumatic/Electric Device:

An external air tank under pressure drives a piston on which, is suspended the test structure. Since the pneumatic system incurs a positive spring stiffness, a linear DC motor is incorporated to introduce a negative spring stiffness to the pneumatic system so that, from the perspective of the test article, the system has very low stiffness. However, such an approach necessitates a very complex control system to insure the proper operation of the suspension device. One such device has been developed under the NASA/LaRC Pathfinder Dynamic Scale Technology Program [2].

(4) Springs:

Different combinations of springs in different configurations have been proposed to introduce a near zero stiffness-rate for the suspension system. However, all such configurations always result in a very small domain of operation (stroke) under which the test structure could move and yet see no constraining force.

The experimental performances of the prior four suspension systems have revealed some inadequacies in their usage. In the case of long cables, the testing is constrained within the horizontal plane while the gravitational effect of the structure is compensated through several long cables. Thus, the entire suspension system must occupy a large space with tall ceilings. In the case of air pads, friction on the horizontal plane may influence the performance of the testing. Moreover, the inertia of air pads may also change the system dynamics particularly when a large number of air pads are used for the large space structure. Moreover, the planar design of air pads constrains the feasibility of testing in the vertical direction. In the case of the pneumatic/electric device [2], a complicated control system is employed to produce a negative spring stiffness. A piston with an external air tank is a cumbersome way when compared to the single cable in this proposed suspension. Furthermore, the controller design must be involved with a linear DC motor to provide the appropriate feedback for the negative stiffness rate. No matter how accurately the output is measured for feedback, the influence of noise upon the dynamic performance cannot be ignored. In the case of springs, the working domain of operation with zero stiffness rate, is strictly limited so that the test structure can move only within a very small stroke.

In the following section the development of a band drive suspension device for testing different test articles will be presented.

3. CONCEPT OF THE BAND DRIVE SUSPENSION SYSTEM

The problem of simulating space environments on earth inspires the development of many suspension systems that can counteract the gravitational effect on test structures, in the vertical direction. A concept based on a band mechanism will be the subject of investigation as to its applicability to dynamic

testing of space structures. These structures will be modelled as lumped, as well as continuous parameter systems and a simulation of the interactive dynamic behavior between the suspension system and structures will be presented.

To begin, figures 2(a) and (b) show two arbitrary positions of a test article in static equilibrium suspended by this suspension device. The suspension device consists of:

(1) a noncircular and specially profiled disk (D),
(2) a torsional spring (S),
(3) a thin cable (C),
(4) a smooth ring (R),
and (5) a test article (W).

Assume that a test article is originally suspended and kept in static equilibrium at the position shown in Fig. 2(a) with the thin cable C wrapped around the edge of the noncircular disk D. This cable passes through the smooth ring R, and extends downwards to suspend the test article W. This smooth ring R may be assumed frictionless. To prevent the cable from driving the disk D and hence unwinding, a torsional spring S is attached to the axis of rotation of the disk D such that the torque exerted on the disk D due to the load imposed by the test article W, is balanced by the torque T_{s_1} in the torsional spring S, i.e.,

$$Wr_1 = T_{s_1} \tag{1}$$

where r_1 is the moment arm which is the perpendicular distance from the disk rotational center to the cable. Then the equilibrium equation of Eq. (1) can be further written as

$$k_s(\theta_{s_0}+\theta_1) = Wr_1 \tag{2}$$

where θ_{s_0} is the angle of preload in the torsional spring S and θ_1 is the of rotational displacement of disk D. Note that this equation provides a explicit relationship between the angle of rotation θ_1 of noncircular disk D and the moment arm r_1. Suppose the test article W is displaced downwards a distance of ι_1 from its original equilibrium position as shown in Fig. 2(a). To enable the test article W to remain in equilibrium at this new position, illustrated in Figure 2(b), the moment arm r_2 subtended at the axis of rotation of the disk D has to be larger than r_1. This is because, to balance the increased torsional spring torque, while the cable is at the same tension W, an increase in the moment arm on the noncircular disk is needed, so that:

$$Wr_2 = T_{s_2} \tag{3}$$

In this new equilibrium position:

$$k_s(\theta_{s_0}+\theta_2) = Wr_2 \tag{4}$$

where θ_2 is new rotational displacement of disk D as illustrated in Fig. 2(b). Note that the moment arms r_1, r_2 are not the radial distances to the points of tangency of the cable at the disk profile, but are the perpendicular distances from the disk rotational axis to the cable. Since the moment arm r_2 is different from r_1, it is then possible to determine the profile of the noncircular disk D such that a continuous change in the moment arm is obtained for any given position of the test article W, in such a way that, when displaced from one position of static equilibrium to other position, the test article will remain in

static equilibrium in its new position. That causes a weightless situation which simulates that in a space environment.

The static characteristic of the suspension system is thus governed by equations (1)-(4). Compared with prior suspension systems discussed in this section where complicated electrical devices or the huge facilities are needed, this band drive suspension system is a rather simple mechanical system. Obviously, the noncircular disk plays a very crucial role in such a suspension system. The profile coordinates of the noncircular disk will be derived by using envelope theory in conjunction with the equilibrium equations given by Eqs. (1)-(4). This will be the subject of discussion in the following section.

4. DESIGN OF THE DISK PROFILE

Envelope theory will be applied to generate the coordinates of the disk profile given in Fig. 3. Using kinematic inversion, an observer, fixed to the disk, would view the sequential positions of the cable which tracks a sequence of straight trajectories $\overline{P_0T_0}$, $\overline{P_1T_1}$, $\overline{P_2T_2}$,..., $\overline{P_nT_n}$ as shown in Fig. 3, as the disk rotates. The swinging point P_i (i=1,2,...,n) is observed to lie on a circular path with a radius r_a which is the distance from the rotational center O to the ring R. These straight trajectories, together when taken infinitesimally apart, gives the envelope which forms the disk profile. Assuming that the initial swinging point P_0 is tangent to both the base circle O and the disk profile, the angle ψ_0 which denotes the starting rotational position of the string is given by:

$$\psi_0 = \sin^{-1}(r_b/r_a) \tag{5}$$

Suppose that the string is viewed by the observer at center O while the disk rotates through an angle θ. Then the thin cable will subtend an angle of $\phi_0+\phi$ with the vertical, at the ring. The increment angle ϕ is the rotational displacement of the string trajectory $\overline{PT}$ from its initial orientation. There therefore exists a relationship between disk rotation θ and the string angular displacement ϕ. This relationship will be derived using the equilibrium equations (2) and (4). From [8], a general equation of the family of lines forming the envelope is governed by a straight line which is:

$$y = mx + b \tag{6}$$

where the slope of the swinging string at disk angular position θ is given by

$$m = \tan(\phi+\phi_0-\theta) \tag{7}$$

and y-intercept of the string $\overline{PT}$ based on the Cartesian system in Fig. 3, is

$$b = r_a\cos(\theta)\tan(\phi+\phi_0-\theta) + r_a\sin(\theta) \tag{8}$$

This general equation of the cable $\overline{PT}$ in Eq. (7) gives a family of strings as a function of the disk angle of rotation θ. From the theory of envelope, an envelope of the family of the straight lines is governed by a equation:

$$\begin{aligned} F(x,y,\theta) &= y - mx - b \\ &= y - \tan(\phi+\phi_0-\theta)[x + r_a\cos(\theta)] - r_a\sin(\theta) \\ &= 0 \end{aligned} \tag{9}$$

Equation (9) is continuous and is a continuously differentiable function in the coordinates x and y as well as in the variable θ. Differentiating the equation (9) with respect to the disk angle θ provides:

$$\partial F/\partial\theta = \tan(\beta)(r_a\sin(\theta)) - [x + r_a\cos(\theta)]\sec^2(\beta)(\partial\phi/\partial\theta-1) - r_a\cos(\theta) = 0 \quad (10)$$

where β equals to $\phi+\phi_0-\theta$. According to [8], the coordinates of disk profile at a given angle θ may be obtained by solving equations (9) and (10), i.e.:

$$x = -r_a[A\sin(\beta) + \cos(\theta)] \quad (11)$$

where

$$A = \frac{\cos(\theta+\beta)}{\partial\phi/\partial\theta-1} \quad (12)$$

Substituting Eq. (11) into Eq. (9) provides

$$y = r_a[-A\sin(\beta) + \sin(\theta)] \quad (13)$$

Initially, the angles θ and ϕ equal zero so that the starting coordinate of the noncircular disk becomes:

$$x = -2r_a\sin(\phi_0/2), \quad (14)$$

$$y = \sin(2\phi_0)/2 \quad (15)$$

which coincides with the point at which the starting string $\overline{P_0T_0}$ is tangent to the base circle in Fig. 3.

The rate of change in orientation of the string as a function of disk rotation $\partial\psi/\partial\theta$ can be determined by investigating the relationship between the angles θ and ϕ. Based on Eq. (2) and illustrated in Fig. 2, the equation of the initial equilibrium is governed by:

$$Wr_a \sin(\phi_0) = k_s \theta_0 \tag{16}$$

For the incremental angles of θ and ϕ, from the initial orientation angles θ_0 and ϕ_0, the new equilibrium state becomes:

$$Wr_a \sin(\phi_0+\phi) = k_s(\theta_0+\theta) \tag{17}$$

Subtracting Eq. (16) from Eq. (17) provides:

$$Wr_a[\sin(\phi_0+\phi)-\sin(\phi_0)] = k_s\theta \tag{18}$$

which can be rewritten as

$$\psi = \sin^{-1}[k_s\theta/(Wr_a)+\sin(\phi_0)]-\phi_0 \tag{19}$$

Differentiating Eq. (19) with respect to the angle θ yields

$$\partial\phi/\partial\theta = \frac{k_s}{Wr_a\cos(\phi_0+\phi)} \tag{20}$$

Then, the profile of the noncircular disk is determined by substituting for ϕ and $\partial\phi/\partial\theta$ in Eqs. (19) and (20) into the equations for the disk coordinates given by equations (11) and (13). Note that the profile of the disk must be convex.

Several parameters are needed to generate the profile of the noncircular disk and they include r_a, r_b, k_s, and W. It can readily be shown that each disk profile can be specified according a parameter which is the ratio of the weight of the test article to the stiffness of the torsional spring, i.e. W/k_s. This means that if testing is to be conducted for another test article twice its original, the torsional spring stiffness must be increased by the same factor so that the same disk can again be used. Such a design therefore permits tremendous flexibility since different loads can be used on this device, without the need to fabricate a new disk every time a new test article with a different mass, is used.

With the disk profile design, the dynamics of the test articles can then be suspended on this band mechanism. The dynamics of these test articles in the presence of a suspension mechanism will be presented in the next section.

5. DYNAMICS OF TEST ARTICLES AND SUSPENSION SYSTEM

In simulating the test experiments of flexible space structures, the test article may be modelled as a discrete or a continuous system. Two models of test articles will be considered: a lumped-parameter model and a continuous parameter flexible steel beam. In the lumped-parameter model, a the test article will be modelled as two masses and a connecting linear spring suspended in equilibrium as shown in Fig. 4(b). Such a lumped-parameter system is thus treated as a simple two-degree-of-freedom discrete system whose flexibility is characterized by the connecting spring. In the continuous parameter model, a flexible steel beam is hung at its two ends and is suspended through two identical disk suspension systems, as shown in Fig. 5. The profile of the noncircular disk in each case is developed through Eqs. (11) and (13) to maintain the static equilibrium of

the test article at any vertical position. Simulation of the ground-based validation testing will be implemented by providing the test article, originally in equilibrium, with the excitations such as an initial displacement or an initial velocity (impulse). The characteristics of flexible space structures are then analyzed together with the band mechanism suspension system.

5.1 Case 1: A Lumped-Parameter Model of a Test Article:

The flexible space structures can be discretized into a series of lumped-parameter elements. The first test structure in Fig. 4(b) illustrates a discrete lumped-parameter system which approximates a flexible structure through the use of two masses and one connecting spring. Table 1 shows the model parameters of such a lumped-parameter system. The band drive suspension system is connected to one of the masses, mass #1. Notice that the mass in Eqs. (16)-(20) stands for the sum of the two masses, so that care is needed while developing the profile of the noncircular disk for this test article. Since this band drive mechanism contains a very nonlinear function within Eqs. (11) and (13), the total system will be a nonlinear two degree-of-freedom dynamic system even though the test article may be a linear system. A derivation of the dynamic equations will be discussed below.

Assume that m_1 and m_2 are the masses of the two rigid bodies, k_2 the spring stiffness between the two bodies, I_c the moment inertia of the disk, k_s the torsional spring rate and, r_a the distance between rotational center O and the ring R. Furthermore, the displacements of the two masses are denoted by ι_1 and ι_2 respectively, while θ and $\dot{\theta}$ denote the angular displacement and angular velocity of the noncircular disk, and ϕ is the displacement angle of the cable. Then from Fig. 4(b), the static equilibrium of the test article at any position is governed by

$$W = (m_1+m_2)g$$
$$= \frac{k_s(\theta+\theta_0)}{r_a\sin(\phi+\phi_0)}$$
$$= \frac{k_s\theta_0}{r_a\sin(\phi_0)} \tag{21}$$

and

$$m_2 g = k_2 \iota_{s_1} \tag{22}$$

where ι_{s_1} indicates the static elongation of the spring, θ_0 is the preloaded angle of torsional spring, and ϕ_0 denotes the initial angular position of the cable. Note that the linear displacement ι_1 of mass m_1 must be consistent with disk angle θ since the suspension cable is directly connected to mass m_1. Due to the convexity of disk profile, the displacement ι_1 in Fig. 4(b) can be equated by integrating along the curvilinear path of the disk profile through the rotation θ so that:

$$\iota_1 = \int_0^{\theta} r_a\sin(\phi+\phi_0)\,d\theta$$
$$= k_s[\theta^2/2 + \theta_0\theta]/W \tag{23}$$

Note that the position ι_1 of mass m_1 is a parabolic function of the disk angle θ. In fact, equation (23) shows a function generator which generates a parabolic curve of the displacement ι_1 in terms of θ. Moreover, differentiating Eq. (23) with respect to time yields

$$\dot{\iota}_1 = [k_s(\theta+\theta_0)/W]\dot{\theta} \tag{24}$$

which indicates the velocity relation between $\dot{\iota}_1$ and $\dot{\theta}$. Therefore, the position and velocity of mass m_1 can be replaced by the disk angle and angular velocity through Eqs. (23) and (24).

Applying Lagrange's equation of motion [9], the Lagrangian function for this system is given by

$$L = T - V \tag{25}$$

where the kinetic energy T and the potential energy V are:

$$T = \{I_c\dot{\theta}^2 + m_1[k_s(\theta+\theta_0)/W]^2\dot{\theta}^2 + m_2\dot{\iota}_2^2\}/2 \ , \tag{26}$$

$$V = k_s(\theta+\theta_0)^2/2 + k_2[k_s(\theta^2/2 + \theta_0\theta)/W - \iota_2 - \iota_{s_2}]/2$$

$$- m_1 g k_s(\theta^2/2 + \theta_0\theta)/W - m_2 g \iota_2 \tag{27}$$

Based on the Lagrangian from Eq. (25), the dynamic equation of motion in matrix form may be written in the following form:

$$\mathbf{M}\ddot{\xi} + \mathbf{K}\xi = \mathbf{f} \tag{28}$$

where ξ denotes the state vector $[\theta \quad \iota_2]^T$. The inertia, stiffness matrices and nonlinear force vector become

$$\mathbf{M} = \begin{bmatrix} I_c + m_1[k_s(\theta+\theta_0)/W]^2 & 0 \\ 0 & m_2 \end{bmatrix} , \tag{29}$$

$$\mathbf{K} = \begin{bmatrix} k_s+k_sk_2(k_s\theta_0^2/W-\iota_{s_1})/W & -k_sk_2\theta_0/W \\ -k_sk_2\theta_0/W & k_2 \end{bmatrix}, \tag{30}$$

$$\mathbf{f} = [\, f_1 \quad f_2 \,]^T, \tag{31}$$

where

$$f_1 = m_1gk_s(\theta+\theta_0)/W-k_s\theta_0+k_sk_2[\theta\iota_2+\iota_{s_1}\theta_0-k_s\theta^3/2/W-$$

$$k_s\theta_0\theta^2/W\ -k_s\theta_0\theta^2/2/W-m_1(k_s/W)^2(\theta+\theta_0)\dot{\theta}^2]$$

and

$$f_2 = k_sk_2\theta^2/(2W)$$

Note that the nonlinearities occur in both the inertia matrix **M** and the nonlinear forcing function vector **f** due to the kinematic nonlinearity arising from the noncircular disk profile. The displacement and velocity of mass #1 may be determined from Eqs. (23) and (24) during the simulation process even though they do not appear explicitly in Eq. (28).

The characteristics of such a lumped-parameter model may then be observed with different initial conditions placed on the lumped masses. For comparison purposes, the dynamic responses of the same test article will be re-simulated using the soft spring suspension system shown in Fig. 4(a). The stiffness of the soft spring has been chosen to be equivalent to the torsional spring rate in the disk suspension system, i.e. $k_1=k_s/r_b^2$. The governing linear dynamic equation for the suspension system in Fig. 4(a) can be found in [10] will not be included in this paper. A second model of the test article is based on a continuous parameter system. The second model will be the subject of investigation in the section below.

5.2 Case 2: Flexible Steel Beam : (A Continuous-Parameter Model)

The band mechanism suspension system may also be applied for the dynamic testing of continuous parameter models of flexible structures as well. Figure 5 demonstrates a uniform rectangular cross-section steel beam hung on two identical disk suspension systems at its two ends. Testing of such a flexible beam is aimed at flexural vibrational behavior. The model parameters of the flexible steel beam are given in Table 2. Assume that the total weight of the flexible beam in static equilibrium is evenly suspended by two identical disk suspension systems. Then, the profile of the noncircular disk is developed using half the weight of the flexible beam when Eqs. (18) and (20) are applied.

Assume that the rigidity of the flexible beam is given by EI product, its density ρ, the length $\bar{L}$, and the displacement of the beam at the left end is denoted by ι_1. The local coordinates x_1-y_1 are located at left end of the flexible beam for determining the local deflection of the beam. The technique of the modal analysis [11,12] will be applied to discretize the beam deflection into a series of flexural modes. The flexible beam deflects during bending vibration about its deformed static equilibrium shape caused by gravity. As will be seen in the simulation of the beam behavior, only odd modes will be excited so that the flexural deflection of this floating hinged-hinged beam in the coordinates x_1-y_1 is symmetrical about its center of this floating gravity. A setup of such a system is shown in Fig. 5.

The flexible beam can be maintained in static equilibrium as long as equations (16) and (17) is satisfied for half the weight of the flexible beam. The displacements and velocities of the flexible beam at two ends can be substituted by the disk angle θ

and angular velocity $\dot{\theta}$ in Eqs. (23) and (24) derived in the lumped-parameter system. For the flexible beam as shown in Fig. 5, the kinetic energy T and the potential energy V can be expressed as:

$$2T = 2I_c\dot{\theta}^2 + \int_0^{\bar{L}} \rho[\ \dot{\mathbf{i}}_1 - \dot{\mathbf{y}}_1\ ].[\ \dot{\mathbf{i}}_1 - \dot{\mathbf{y}}_1\ ]dx_1, \tag{32}$$

$$2V = 2k_s[\theta+\theta_0]^2 + \int_0^{\bar{L}} EI\{\ \mathbf{y}_{1,x_1x_1}\}^2\ dx_1 \tag{33}$$

where $\mathbf{x}_1$ is a vector at the root end, and is tangent to the longitudinal x_1 axis of the flexible beam. Moreover, the distributed coordinates are expanded in an orthogonal basis of assumed mode shapes so that:

$$\mathbf{y}_1(x_1,t) = \psi^T(x_1)\ \mathbf{q}(t),$$
$$\psi^T = [\psi_1,\ldots,\psi_n] \qquad \text{and} \qquad \mathbf{q}^T = [q_1,\ldots,q_n] \tag{34}$$

where $\psi(x_1)$ is a vector of assumed mode shapes relative to a spatial coordinates derived from the hinged-hinged boundary condition problem, $\mathbf{q}(t)$ is a generalized coordinate vector [11,12], and n is the number of assumed modes.

Inserting Eq. (34) into Eqs. (32) and (33) yields

$$2T = 2I_c\dot{\theta}^2 + \rho\bar{L}\dot{i}_1^2 + \sum_{i=1}^{n}\sum_{j=1}^{n} m_{ij}\dot{q}_i\dot{q}_j - 2\sum_{i=1}^{n} h_i\dot{q}_i\dot{i}_1, \tag{35}$$

$$2V = 2k_s[\theta+\theta_0]^2 + \sum_{i=1}^{n}\sum_{j=1}^{n}\kappa_{ij}q_iq_j \tag{36}$$

where

$$m_{ij} = \int_0^{\bar{L}} \rho \psi_i(x_1)\psi_j(x_1)\, dx_1,$$

$$P_i = \int_0^{\bar{L}} \rho x_1 \psi_i(x_1)\, dx_1,$$

$$h_i = \int_0^{\bar{L}} \rho \psi_i(x_1)\, dx_1,$$

$$\kappa_{ij} = \int_0^{\bar{L}} EI\psi_{i,x_1x_1}\psi_{j,x_1x_1}\, dx_1 \qquad \text{for } i,j=1,2,\ldots,n$$

Therefore, the Lagrangian for the system, as given by Eq. (25), can then be obtained. From Eqs. (35) and (36), the displacement and velocity at the beam ends are converted into the angular displacement and angular velocity of the disk. To simplify the state variables in the above equations, denote $\xi_0=\theta$, $\xi_i=q_i$, for $i=1,2,\ldots,n$. Using the Lagrange's equations of motion [9], the equation of motion of the system may be written as:

$$\mathbf{M}\ddot{\xi} + \mathbf{K}\xi = \mathbf{f} \tag{37}$$

where the state vector $\xi^T=[\theta,q_1,q_2,\ldots,q_n]$. The inertia matrix **M**, the stiffness matrix **K** and the nonlinear force vector **f** are given by:

$$\mathbf{M} = \begin{bmatrix} 2I_c+4\rho\bar{L}(k_s/W)^2[\theta+\theta_0]^2 & -2k_s[\theta+\theta_0]\mathbf{h}^T/W \\ \textbf{symmetric} & \rho\bar{L}\hat{\mathbf{I}} \end{bmatrix}, \tag{38}$$

$$\mathbf{K} = \text{Diag}\ [\ 0,\ \rho\bar{L}\omega^2\ ]\ ;\quad \omega = \text{Diag}\ [\ \omega_1,\ldots,\ \omega_n\ ]\ , \tag{39}$$

$$\mathbf{f} = \begin{bmatrix} -4\rho\bar{L}(k_s/W)^2[\theta+\theta_0]\dot{\theta}^2 \\ 2k_s\dot{\theta}^2\mathbf{h} \end{bmatrix} \tag{40}$$

where $\hat{\mathbf{I}}$ is an n×n identity matrix and ω_i (i=1,...,n) are the modal frequencies associated with the hinged-hinged shape functions $\psi_i(x_1)$, used in discretizing the deflection of the flexible beam. The nonlinearities of the system all reside within the inertia matrix and the nonlinear force vector. The displacement and velocity at the ends of the beam can be computed directly from Eqs. (23) and (24) during the simulation. In this way, symmetric motions of the flexible beam may then be tested using two identical disk suspension systems.

6. SIMULATION RESULTS

The dynamics of test articles have been derived in the previous section, and they include a lumped-parameter system as well as a continuous-parameter system. One disk suspension system is required for the lumped-parameter system while two identical disk suspension systems are needed to suspend the flexible beam at its two ends. For each test article, two different excitations to the system will be implemented. The first is with an initial displacement and the second, with an initial velocity; with a total of four simulations to verify the feasibility of this disk suspension system. A soft spring will be employed as a suspension system (see Fig. 4(a)) for the lumped-parameter system and its simulations are then compared to those on the disk suspension system.

The parameters of disk suspension system which will be used for simulations are shown in Tables 1 and 2. A convex profile of noncircular disk is then drawn by evaluating Eqs. (11) and (13).

Figure 6 shows the resulting profile of the noncircular disk with several spokes which can eliminate its moment of inertia. The disk radius varies from 3 inch to 9.5 inch. In the middle of disk thickness, a curvilinear groove is cut along the edge of disk for the winding cable. The range along the disk edge allows the disk rotate about 200 degrees. Such a noncircular disk in Fig. 6 will be used to implement the following dynamic simulations.

6.1 Simulations of the Lumped-Parameter Model:

Table 1 summarizes the model parameters of a lumped-parameter system. Two kinds of suspension systems, a band mechanism and spring suspension system, will be used. In both types of suspension systems, the test article is hung in static equilibrium by connecting mass #1 to the suspension system through a thin cable. In the first simulation, -0.2 inch and 0.2 inch of initial displacements are specified to masses #1 and #2 respectively but with no initial velocity. Figures 7(a)-(f) are the simulation results of the two suspension systems. The results associated with the disk suspension system are indicated by a solid line while those of spring suspension system, by a dotted line. Figures 7(a) and 7(b) show the angular displacement and angular velocity of the disk respectively of the disk suspension system. Both angular displacement and angular velocity oscillate with the natural frequency of the test article. The displacement and velocity of mass #1 are respectively shown in Figs. 7(c) and 7(d), while the displacement and velocity of mass #2 are given in Figs. 7(e) and 7(f) respectively. All the trajectories of masses #1 and #2 represent pure oscillatory motions about their equilibrium positions. The cable which connects the test article and the disk is found always in tension. It can be seen that there is no difference between disk suspension system and the simple spring system under specifications of initial displacements. The spring in the spring system may be too soft

due to the equivalent relationship, $k_1=k_s/r_b^2$ so that it may not be able to suspend heavy test articles. The spring stiffness for this spring suspension system cannot be arbitrarily increased because, that will distort the natural frequency of the test article. The initial-displacement results provide an insight in verifying the validity of disk suspension system when compared to the conventional spring suspension system. It also shows that the results correspond to the anticipated vibrational characteristics of mass #1 and #2 in space, as well.

The second simulation of a lumped-parameter system deals with the dynamic response subjected to initial velocity specification. An initial velocity of 2 inches per second acts on mass #2 to excite the whole system to move as if under an impulse. Figure 8(a) shows the dynamic history of the disk angle. It has an oscillatory motion superimposed on the dropping angular displacement trajectory. Figure 8(b) illustrates this oscillatory motion of the disk but with an average angular velocity 9.5 deg/sec superimposed upon that oscillation. The displacements and velocities of masses #1 and #2 are shown in Figs. 8(c)-(f). In Figs. 8(c) and 8(e), the solid lines associated with disk suspension system show that the entire test article is dropping at a constant velocity while masses #1 and #2 which model the test article are oscillating during this downward motion. This shows that the impulse response indeed corresponds to that in a zero-gravity condition, with the use of this disk suspension system. Figures 8(c) and 8(e) also show that the spring suspension system on the other hand, does not satisfy this anticipated motion trajectory of the test article (masses). The velocities of masses shown in Fig. 8(d) and 8(f), confirm that the masses in the disk suspension system on the average, do not accelerate. The pure oscillations of both the mass velocities indicate an average constant velocity of 1 in/sec rather than zero implying that the constant velocities are indeed due to the

impulse response. This implication shows that the entire test article beneath the disk suspension system is not accelerated due to the initial impulse. Such a phenomenon is consistent with the behavior deduced from mass displacements in Fig. 8(c) and 8(e). Note that the masses oscillate at 180 degrees out of phase with each other. These figures also show that the simple spring suspension system do not result in a correct motion for the masses in response to an initial impulse.

Figures 9(a)-(f) thus ensure that this disk suspension system is capable of simulating the dynamic behavior of the test article subjected to an impulse. The test body accordingly translates at a constant velocity. When the mass is imposed with an initial velocity V_0, (equivalent to an impulse) the test article will continue to travel at that same velocity V_0 over a considerable range of travel. This is because the tension in the cable is constant and is exactly equal to the weight of the test article, so that there is no net driving force on the article during its entire range of motion. With that observation, it therefore leads to a constant velocity of the test article and in so doing, exactly simulates the motion of an object in space.

6.2 Simulations of the Flexible Steel Beam:

In this simulation experiment, two identical disk suspension systems are employed to suspend a flexible beam that has the same weight as in the lumped-parameter model of the previous section. The model parameters of a flexible steel beam are listed in Table 2. Three hinged-hinged flexible modes will be assumed for the flexible steel beam. In this simulation, the first and third modes will be specified with initial values. This means that the flexible beam is originally bent into a symmetric deformed configuration about its static equilibrium configuration, and then released from rest. Hence, the first and third modes are

excited by this initial deformation. The simulation results are given in Figs. 9(a)-(f). Figures 9(a) and 9(b) displacement and angular velocity of the disk while figures 9(c) and 9(d), the deflection and velocity of the beam at its center of gravity. Figures 9(e) and 9(f) on the other hand, show the deflection and velocity of the beam at both ends of the beam. The rotation of the disk is consistent with the flexural vibration of the beam at the two ends. The odd modes, as anticipated, are very active as can be seen from results of displacement and velocity in the figures. This is due to the symmetry of the deflection about a plane through the center of gravity of the beam. In Fig. 9(c), the displacement at beam's c.g. implies that the beam oscillates about its original static equilibrium configuration during the process. Hence, the multi-mode vibration of a flexible beam can be implemented under the disk suspension system.

Finally, a fourth simulation has been conducted with the flexible beam subjected to an initial impulse. Simulation results are shown in Figs. 10(a)-(f) including the disk angle, angular velocity of disk, beam's c.g. displacement and velocity, and beam's end displacement and velocity. The third mode is more pronounced in the velocity plots and the amplitude of beam's deflection at the center of gravity is larger than those at both ends. The linear slope in the oscillatory behavior in Figs. 10(c) and 10(e) indicates a constant-speed motion associated with a rigid-body mode. The flexible beam is moving upwards at a constant speed while simultaneously vibrating with respect to the local coordinates x_1-y_1. The constant speed is approximately 0.7 in/sec. In fact, these impulse results of a beam implies a compound motion of the flexible space structure that includes a constant-speed rigid-body motion with flexible-body vibration superimposed on it.

The impulse response of a flexible structure has shown to be consistent in the use of this disk suspension device. The entire

test structure will travel at a constant velocity with a rigid-body motion while the traveling beam oscillates, with its flexible modes about the moving local coordinate system. The similarities of the second and fourth simulation results validates the applicability of this disk suspension system for both discrete and continuous models.

7. CONCLUSION

This paper has presented a band mechanism that is to be used as a ground-based suspension system to assess the characteristics of flexible space structures that operate in a weightless environment. This mechanism is characterized by a noncircular disk with a convex profile constrained into rotational motion, by a torsional spring. The suspension system is constructed to counteract the weight of the test article by using a specially shaped disk in conjunction with an appropriate torsional spring. The basic principle behind this suspension system is to maintain static equilibrium of the test article at any given vertical position. The convex profile of the disk is determined using envelope theory. It has also be shown that this suspension system is applicable for test articles with the different weights without the need to change the disk profile; the torsional spring rate has to be adjusted to maintain the static equilibrium condition of the new test article.

This mechanism has shown, under numerical simulation, to be applicable and suitable for ground-based dynamic testing of test articles, be they discrete or continuous models. Two kinds of test articles have been chosen for the simulation, a lumped-parameter system and a flexible steel beam. The lumped-parameter element is composed of two masses and a connecting spring which provides a single-mode vibration. Simulation results indicate that the characteristics of the flexible space structures can be precisely tested under this disk suspension system. It has also

shown to be capable of permitting a constant-speed motion superimposed with flexural vibration in an impulse response. These simulation results provide very useful insights in building up the experimental equipment at NASA-Langley.

ACKNOWLEDGEMENT

The first and second authors wish to acknowledge the support of this investigation through NASA Grant No. NAG1-830 from the Spacecraft Dynamics Branch at NASA Langley Research Center.

REFERENCES

1. Harvey, T.J., "A Second Generation Zero Spring Rate Support System," AIAA/AFOSR Workshop on Microgravity Simulation in Ground Validation Testing of Large Space Structures, Nov. 1-2 1989, Denver, Colorado.

2. Kienholz, D.A., "A Pneumatic/Electric Suspension Device for Very Low Frequency Dynamic testing," AIAA/AFOSR Workshop on Microgravity Simulation in Ground Validation Testing of Large Space Structures, Nov. 1-2 1989, Denver, Colorado.

3. Lynn, P., "Zero Gravity Suspension Systems," AIAA/AFOSR Workshop on Microgravity Simulation in Ground Validation Testing of Large Space Structures, Nov. 1-2 1989, Denver, Colorado.

4. Quartararo, R. and Hasselman, T.K., "Development of a Microgravity Suspension System," AIAA/AFOSR Workshop on Microgravity Simulation in Ground Validation Testing of Large Space Structures, Nov. 1-2 1989, Denver, Colorado.

5. Gronet, M.J., Brewster, R.G. and Crawley E.F., "Assembly and suspension Issues for the DSMT Pathfinder Scale Model," AIAA/AFOSR Workshop on Microgravity Simulation in Ground Validation Testing of Large Space Structures, Nov. 1-2 1989, Denver, Colorado.

6. Colley, V.M., "Large Motion Suspension Devices for Flexible Structures," AIAA/AFOSR Workshop on Microgravity Simulation in Ground Validation Testing of Large Space Structures, Nov. 1-2 1989, Denver, Colorado.

7. Janiszewski, M.A., "Structural Testing Using the KC-135 In-flight Microgravity Simulation facility," AIAA/AFOSR Workshop on Microgravity Simulation in Ground Validation Testing of Large Space Structures, Nov. 1-2 1989, Denver, Colorado.

8. Chen, F.Y., Mechanics and Design of Cam Mechanisms, Pergamon Press, New York, 1982.

9. Greenwood, D.T., Principles of Dynamics, Prentice-Hall, Inc., Englewood Cliffs, New Jersey.

10. Meirovitch, L., Analytical Methods in Vibrations, Third Printing, MacMillan Company, New York, N.Y., 1971.

11. Huang, J.-K., Yang, L.-F. and Juang, J.-N., "Large Planar Maneuvers for Articulators Flexible Manipulators", Proceedings of the Guidance, Navigation and Control Conference, AIAA paper No. 88-4119, August 1988.

12. J.-N. Juang, L.-F. Yang and J.K. Huang, "Lyapunov-based Control Designs for Flexible-Link Manipulators", AIAA/ASME/ASCE/AHS 30th Structures, Structural Dynamics and Materials Conference, Mobile, Alabama, April 5-7, 1989.

Table 1: Parameters of a lumped-parameter model with disk suspension system

(a) Disk suspension system:					
r_a	= 12	in	r_b	= 6	in
k_s	= 0.5	lb/rad	I_c	= 0.01	lb-in^2
(b) Test article: (A lumped-parameter model)					
m_1	= 12	lb	m_2	= 12	lb
k_2	= 1	lb/in			

Table 2: Parameters of a flexible steel beam with disk suspension systems

(a) Disk suspension systems:					
r_a	= 12	in	r_b	= 6	in
k_s	= 0.5	lb/rad	I_c	= 0.01	lb-in^2
(b) Test article: (A flexible steel beam)					
$\bar{L}$	= 6.562	ft			
EI	= 74.8953	lb-ft^2			
ρ	= 0.30480	lb/in			
h	= 1.614×10^{-2}	in			

NOMENCLATURE

A	: parameter for disk coordinates
b	: y-intercept of a general straight line
C	: cable
D	: noncircular disk
EI	: rigidity
F	: a continuous function of envelope theory
f	: nonlinear force vector
f_1	: first element of force vector **f**
f_2	: second element of force vector **f**
g	: gravitational constant
I_c	: moment inertia of noncircular disk
K	: stiffness matrix
k_s	: torsional spring stiffness
k_1	: spring stiffness within the soft spring suspension system
k_2	: spring stiffness of a linear spring
L	: Lagrangian
$\bar{L}$	: length of the beam
M	: inertia matrix
m	: slope of a general straight string
m_1, m_2	: two masses associated with two rigid bodies
n	: number of vibrational modes
O	: disk rotational center
q(t)	: generalized coordinate vector
R	: smooth ring
r_a	: distance between rotational center and ring
r_b	: original length of a swinging string
r_1, r_2	: moment arms of noncircular disk
S	: torsional spring

T : kinetic energy

T_{s_1}, T_{s_2} : torques due to loading from test structures

V : potential energy

V_0 : initial velocity

W : weight of test structure

x, y : coordinates of disk profile

x_1 : x coordinate of the local beam coordinate

$y_1(x_1,t)$: y coordinate of the local beam coordinate

$\mathbf{x_1}, \mathbf{y_1}$: vectors tangent to x_1-y_1 coordinates

ϕ : rotational displacement of the string $\overline{PT}$

ϕ_0 : initial orientation of the string $\overline{PT}$

$\psi(x_1)$: vector of mode shapes

$\boldsymbol{\iota_1}$: vector along the displacement ι_1

ι_{s_1} : initial elongation of a linear spring

ι_1, ι_2 : positions of two masses

$\dot{\iota}_1$, $\dot{\iota}_2$: velocities of two masses

θ : angular displacement of disk

θ_{s_0} : initially preloaded disk angle

θ_0 : preloaded angle of torsional spring

$\dot{\theta}$: angular velocity of disk

ξ : state vector

ω : modal frequency vector

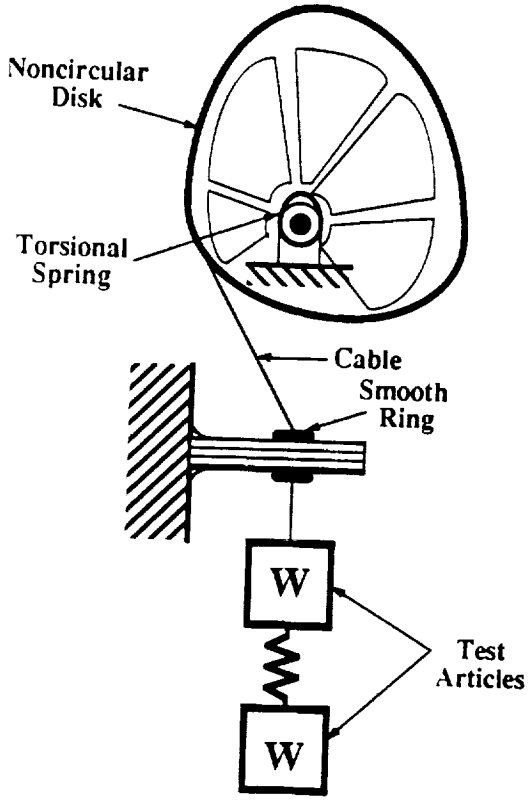

Figure 1: Disk suspension system

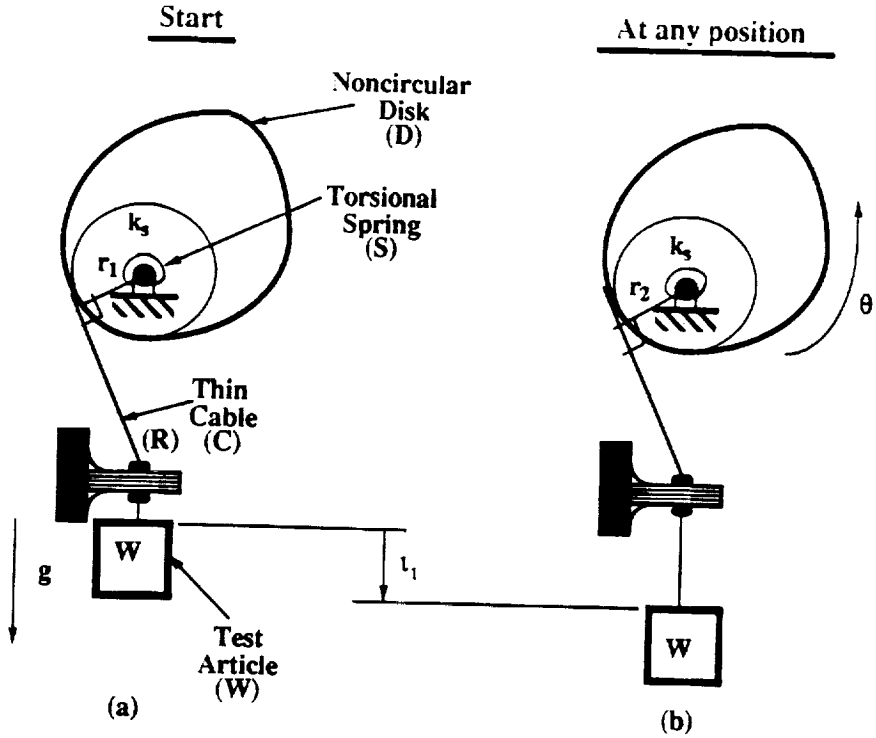

Figure 2: Static equilibrium of a test article at two different positions under disk suspension system

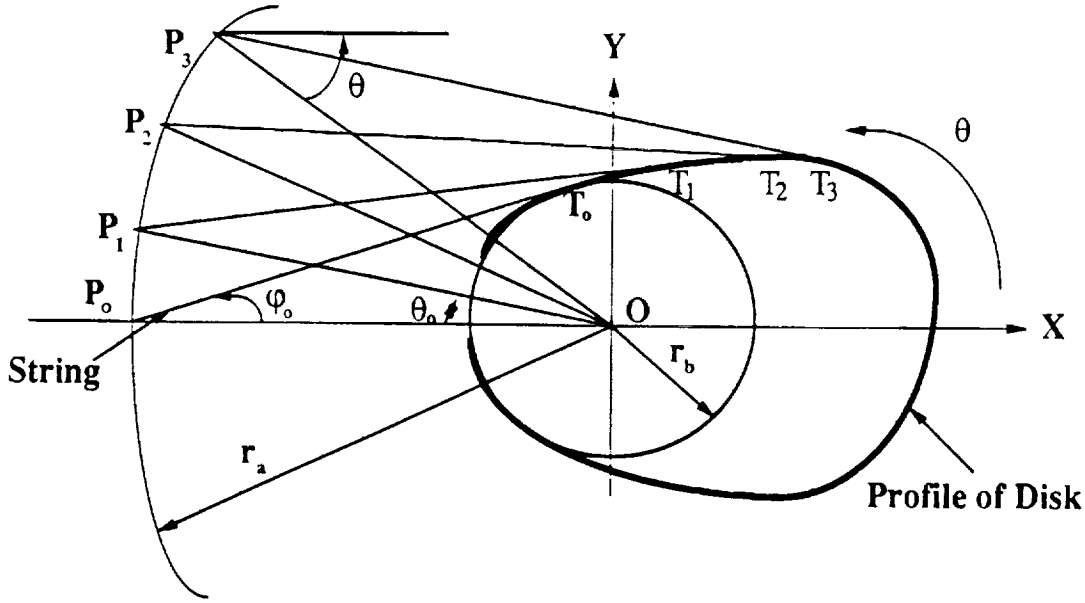

Figure 3: Development of noncircular disk profile

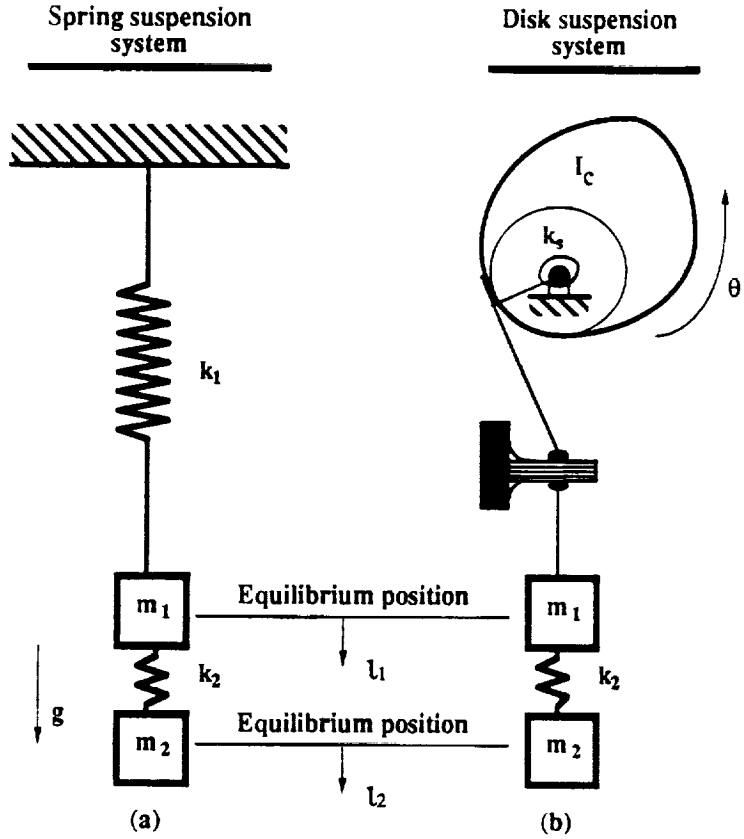

Figure 4: A lumped-parameter model

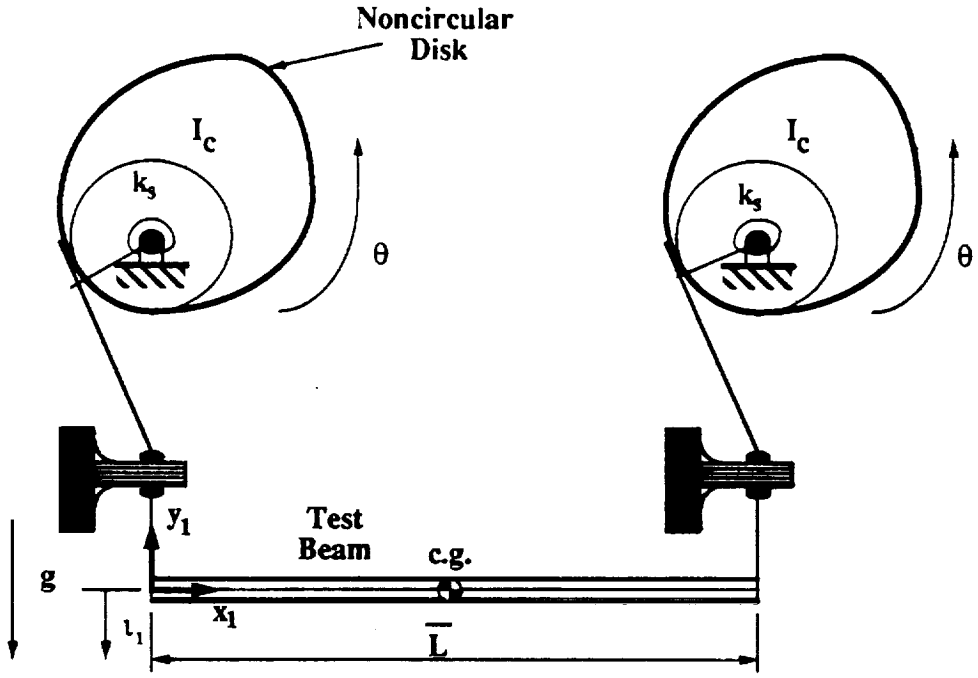

Figure 5: A flexible steel beam

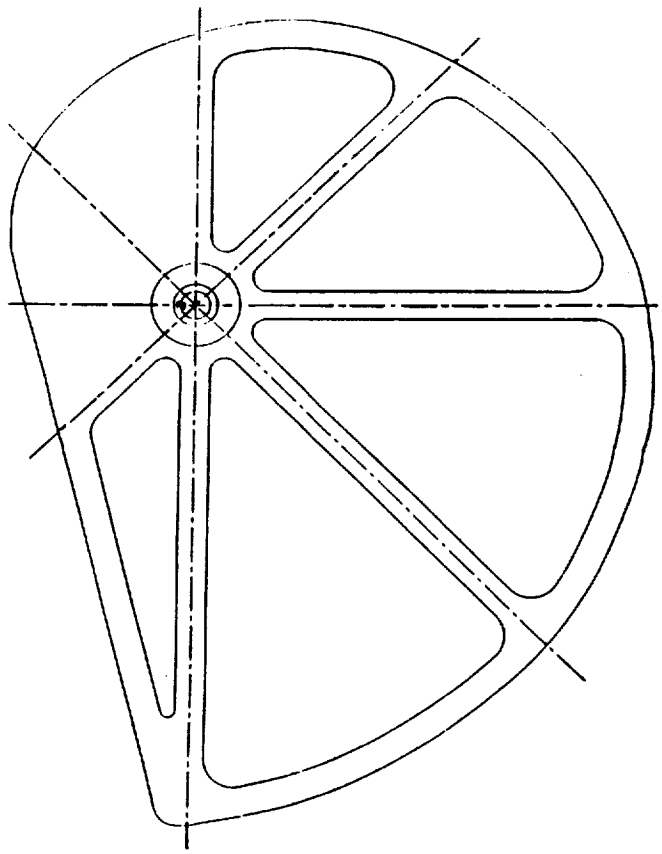

Figure 6: Profile of noncircular disk

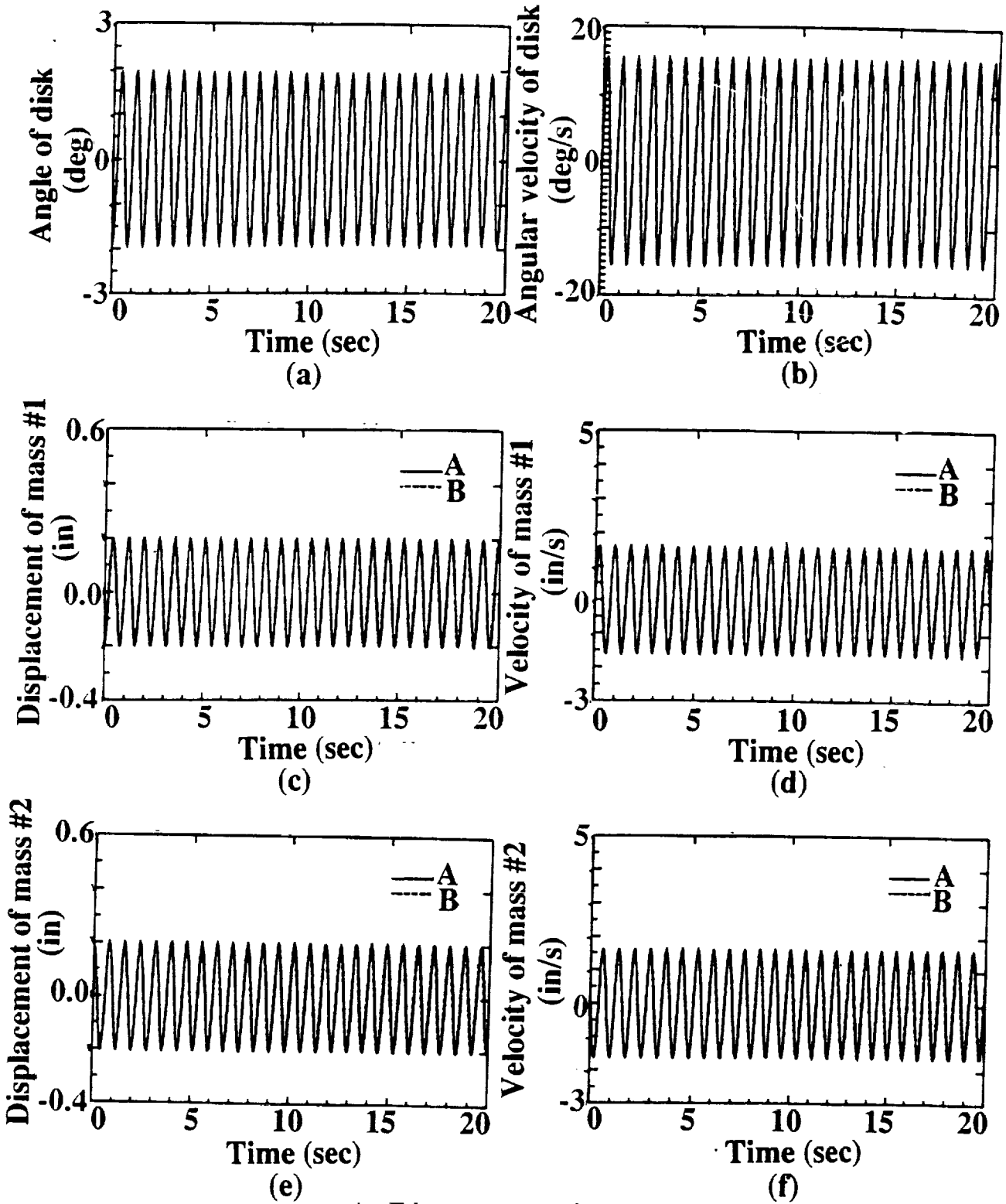

A: Disk suspension system
B: Spring suspension system

Figure 7: Simulation results of a lumped-parameter model for the excitation of the initial displacement

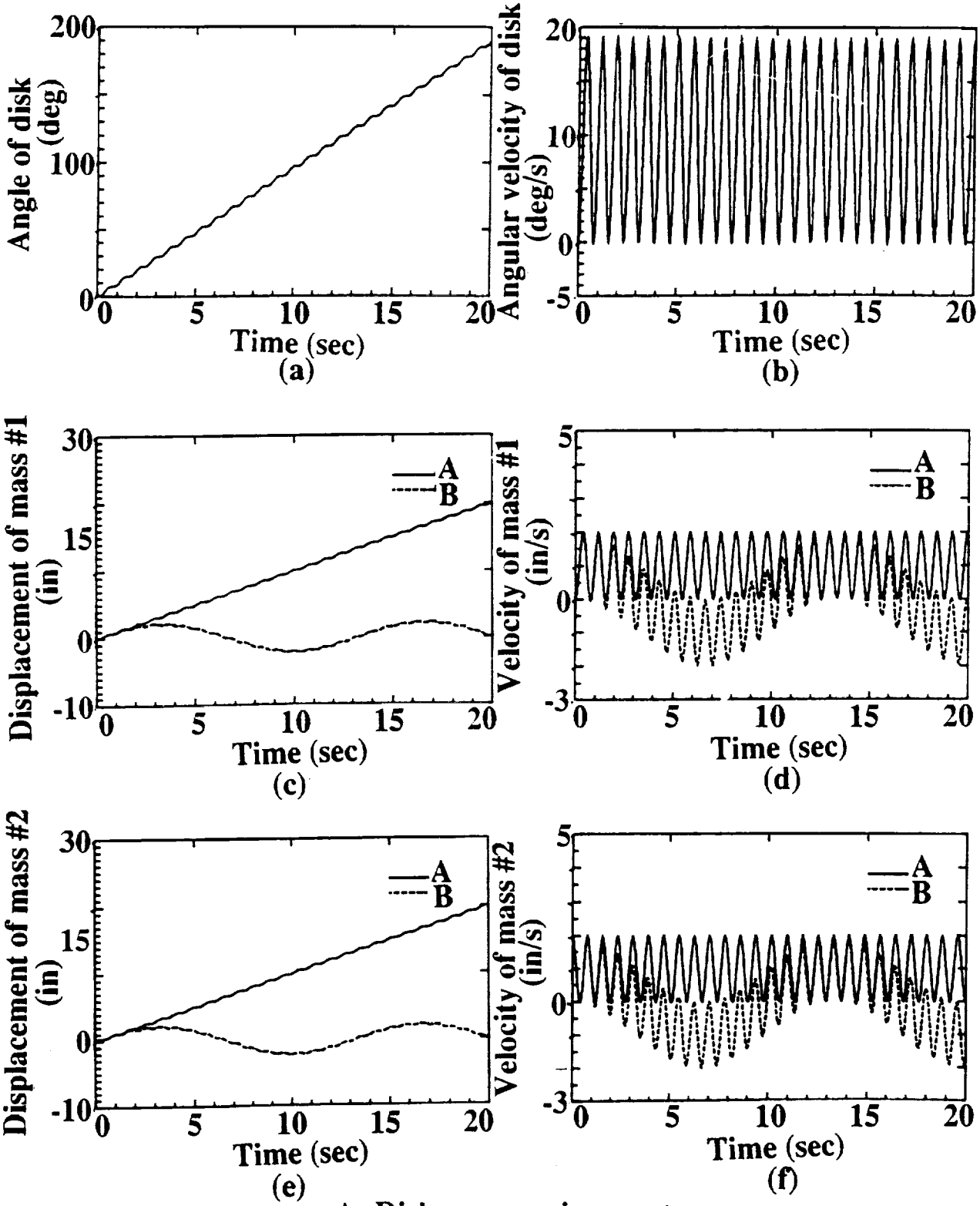

A: Disk suspension system
B: Spring suspension system

Figure 8: Simulation results of a lumped-parameter model for the excitation of the initial velocity

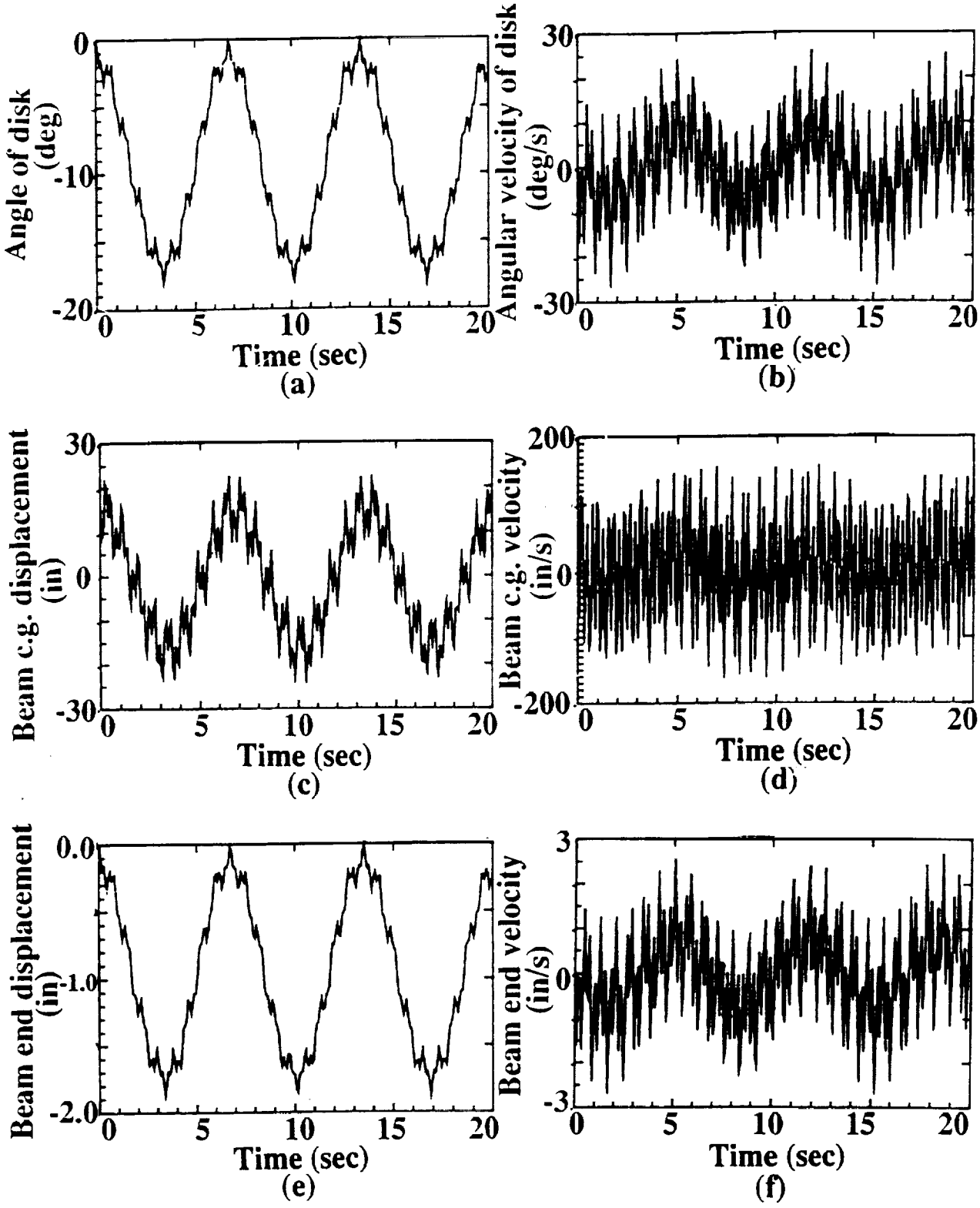

Figure 9: Simulation results of a flexible steel beam for the excitation of the initial displacement

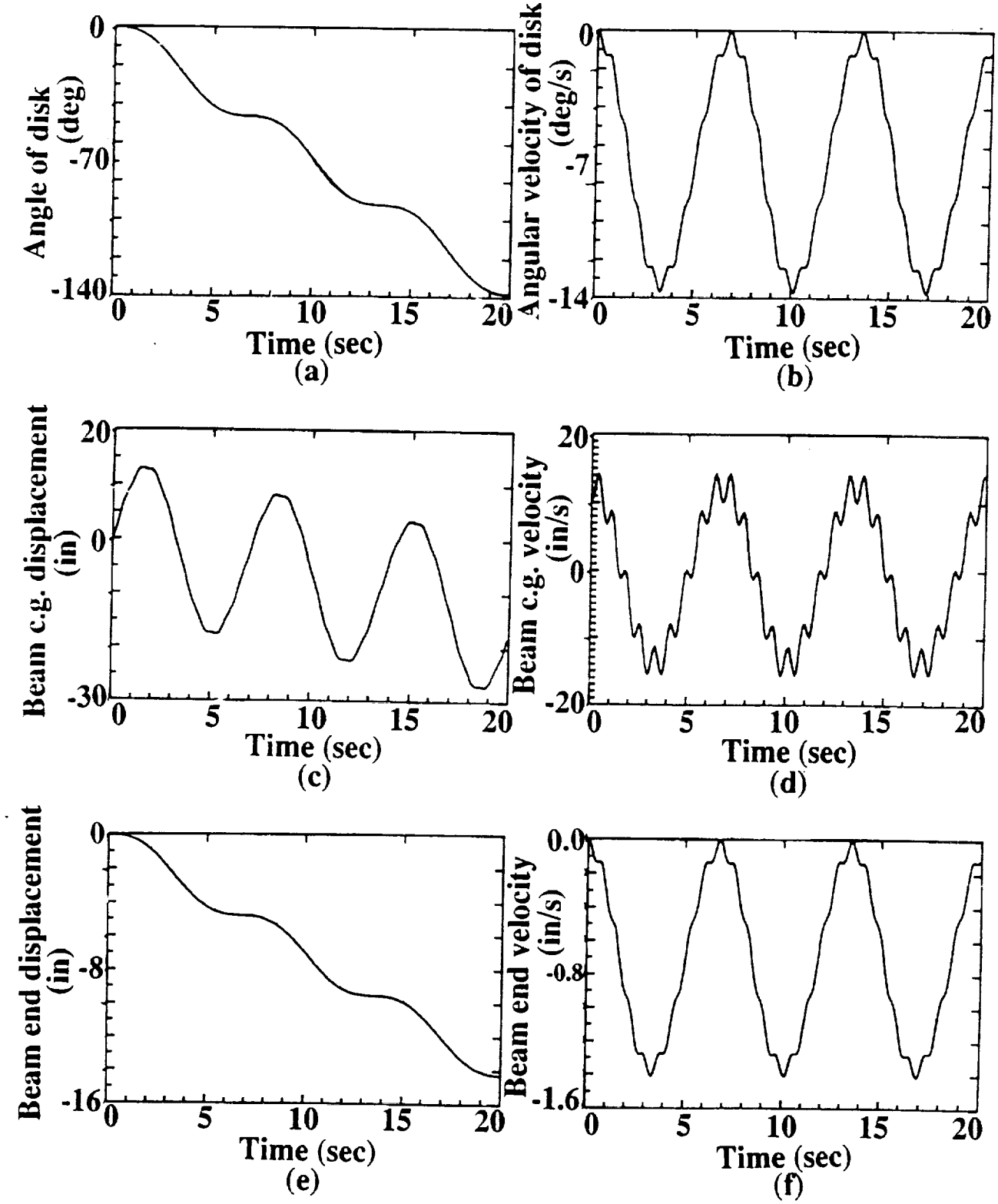

Figure 10: Simulation results of a flexible steel beam for the excitation of the initial velocity